Contemporary circulating enterovirus D68 strains show differential viral entry and replication in human neuronal cells

David M Brown[1], Alison M Hixon[2], Lauren M Oldfield[1], Yun Zhang[3], Mark Novotny[3], Wei Wang[1,#a], Suman R. Das[1,#b], Reed S Shabman[1,#c], Kenneth L Tyler[4,5,6], Richard H Scheuermann[3,7*]

[1]J. Craig Venter Institute, Rockville, Maryland, United States of America

[2]Neuroscience Program and Medical Scientist Training Program, University of Colorado School of Medicine, Aurora, Colorado, United States of America

[3]J. Craig Venter Institute, La Jolla, California, United States of America

[4]Department of Neurology, University of Colorado School of Medicine, Aurora, Colorado, United States of America

[5]Denver VA Medical Center, Denver, Colorado, United States of America

[6]Departments of Immunology and Microbiology, and Medicine, University of Colorado School of Medicine, Aurora, Colorado, United States of America

[7]Department of Pathology, University of California, La Jolla, California, United States of America

[#a]Current address: Viral Immunology Section, NIAID-NIH, Bethesda, Maryland, United States of America

[#b]Current address: Department of Medicine, Vanderbilt University School of Medicine, Nashville, Tennessee, United States of America

[#c]Current address: American Type Culture Collection (ATCC), Gaithersburg, Maryland, United States of America

* Corresponding author

E-mail: RScheuermann@jcvi.org

Short Title: Neuronal cell tropism of EV-D68

Abstract

Historically, enterovirus D68 (EV-D68) has primarily been associated with respiratory illnesses. However, in the summers of 2014 and 2016 EV-D68 outbreaks coincided with a spike in polio-like acute flaccid myelitis/paralysis (AFM/AFP) cases. This raised concerns that the EV-D68 virus could be the causative agent of AFM during these recent outbreaks. To assess the neurotropic capacity of EV-D68, we explored the use of the neuroblastoma-derived neuronal cell line, SH-SY5Y, as a tissue culture model to determine if differential infection permissibility is observed for different EV-D68 strains. In contrast to HeLa and A549 cells, which support viral infection of all EV-D68 strains tested, SH-SY5Y cells only supported infection by a subset of contemporary EV-D68 strains, including members from the 2014 outbreak. Viral replication and infectivity in SH-SY5Y was assessed using four different assays – infectious virus production, cytopathic effects, cellular ATP release, and VP1 capsid protein production – with similar results. Similar differential neurotropism was also observed in differentiated SH-SY5Y cells, primary human neuron cultures, and a mouse paralysis model. Using the SH-SY5Y cell culture model, we determined that barriers to viral entry was at least partly responsible for the differential infectivity phenotype, since transfection of genomic RNA into SH-SY5Y generated virions for all EV-D68 isolates, but only a single round of replication was observed from strains which could not directly infect SH-SY5Y. In addition to supporting virus replication and other functional studies, this cell culture model may help confirm epidemiological associations between EV-D68 strains and AFM and allow for the rapid identification of emerging neurotropic strains.

Author Summary

Since the outbreak during the summer of 2014, EV-D68 has been linked to a type of limb paralysis referred to as acute flaccid myelitis (AFM), with evidence mounting for the causal link of EV-D68 to AFM. Among these AFM cases, concurrent EV-D68 infection was confirmed in several independent epidemiological clusters in four continents. In this report, we describe a neuronal cell culture model (SH-SY5Y cells) where only a subset of contemporary 2014 outbreak strains of EV-D68 show infectivity in neuronal cells, or neurotropism, based on four different assays of viral replication and infection. We further confirmed the observed difference in neurotropism *in vitro* using primary human neuron cell cultures and *in vivo* with a mouse paralysis model. Using the SH-SY5Y cell model, we determined that a barrier to viral entry is at least partly responsible for neurotropism. SH-SY5Y cells may be useful in determining if specific EV-D68 genetic determinants are associated with neuropathogenesis, and replication in this cell line could be used as rapid screening tool for identifying neurotropic EV-D68 strains. This may assist with better understanding of pathogenesis and epidemiology, and with the development of potential therapies.

Introduction

The *Enterovirus* genus in the *Picornaviridae* family comprises many important human pathogens, including human rhinoviruses (HRV), the most common viral agents of the common cold; polioviruses, the causative agent of poliomyelitis; enterovirus A71 (EV-A71), associated with a variety of neurological diseases; and enterovirus D68 (EV-D68). Enteroviruses appear to continually circulate in human populations, with most infections being asymptomatic. For example, up to 72 percent of poliovirus infections are asymptomatic [1]. When poliovirus infections are symptomatic, they can cause a wide spectrum of clinically-distinct syndromes, ranging from minor, non-specific illness, to non-paralytic aseptic meningitis and flaccid paralysis [2]. Before the widespread use of effective vaccines, poliovirus-induced paralysis reached a peak of 21,000 cases in the U.S. in 1952 [3].

EV-D68 was first detected in children with pneumonia and bronchiolitis in 1962 [4]. Until recently, EV-D68 was one of the most rarely reported enteroviruses, with only 26 cases documented by the National Enterovirus Surveillance System in the U.S. from 1970 to 2005 [5]. Beginning in 2009, multiple contemporary clades began emerging worldwide [6]. In the summer and fall of 2014, 49 U.S. states experienced a nationwide outbreak of severe respiratory illness associated with EV-D68, with 1,153 confirmed cases, including 14 deaths [7]. Shortly after the U.S. outbreak, EV-D68 infections were also reported in Canada, Europe, and Asia. The total number of reported EV-D68 cases in 2014 exceeded 2,000 from 20 countries, resulting in the public health community classifying EV-D68 as a re-emerging pathogen of public health concern [8].

Reports of acute flaccid myelitis (AFM) occurring coincident to the outbreak of respiratory disease attributed to EV-D68 raised the possibility that EV-D68 might be the causative agent [7]. EV-D68 infection within a subset of these AFM cases was confirmed in several independent epidemiological clusters in the U.S. [9-14], France [15], Norway [16] Canada [17] and Australia [18]. Statistical analyses of the AFM cases in Colorado [12] and California [19] have supported the association between EV-D68 and AFM, and viral nucleic acid detection studies of patient samples have failed to reveal an alternative etiology [7, 10]. During the 2014 EV-D68 outbreak, patients presenting with AFM showed distinctive magnetic resonance imaging (MRI) findings characterized by brain stem and gray matter longitudinally extensive spinal cord lesions. This matches the findings described in previous outbreaks of EV-A71-associated AFM [9, 19, 20], suggesting that an enterovirus may be responsible. In support of this hypothesis, Hixon *et al.* [21] established that several contemporary EV-D68 strains, but not the historically archetypal Fermon and Rhyne EV-D68 strains, can cause a paralytic disease in neonatal mice due to viral infection and killing of spinal cord motor neurons.

Phylogenetic analysis reported that many of the 2014 EV-D68 outbreak isolates associated with AFM appeared to belong to the phylogenetic subclade, B1 [10, 22]. Interestingly, 12 substitutions identified in B1 2014 isolates carry the same amino acid or nucleotide residues observed at equivalent positions in other paralysis-causing enteroviruses, including poliovirus and EV-A71 [22]. This suggests that one or more of the nucleotide substitutions present in contemporary EV-D68 strains and lineages and

not found in historical archetypal strains, may be responsible for the apparent increased incidence of neuropathology associated with the 2014 outbreak. EV-D68 has continued to evolve since the 2014 outbreak, which is unsurprising as mutation and recombination are known to occur in enteroviruses [23, 24]. Sequence analysis has led to the classification of a new clade D (a subclade of A) [25, 26], and a new subclade, B3, has emerged and quickly expanded [25, 27, 28]. Neurological symptoms have been associated with the novel B3 clade in Sweden [29], the Netherlands [30], Taiwan [31], Italy [32] and the United States [33] which experienced another AFM outbreak during the 2016 enterovirus season (summer and fall), with a total of 149 confirmed cases [2]. The seasonality and magnitude of this AFM outbreak matches the AFM surge observed in 2014. Additional surveillance of potentially emerging neurotropic or neuropathogenic strains is warranted.

To test if a specific genotype is associated with neurological symptoms, we report the development of a cell culture infection model based on the neuroblastoma cell line SH-SY5Y, that shows differential infectivity by different EV-D68 isolates. We observe a correlation between infection and replication in SH-SY5Y cells and neuropathogenesis in mice. This neuronal SH-SY5Y model may be useful for analysis of virus-host interactions *in vitro* and provides a facile assay to quantify which EV-D68 strains are neurotropic and neuropathogenic, potentially leading to better surveillance of virulent EV-D68 strains.

Results

SH-SY5Y cells express higher levels of neuron-specific genes than other candidate cell lines

Seeking a human cell culture to model neuron-specific infectivity, we performed expression profiling of two commonly used 'neuronal-like' cell lines, SH-SY5Y and HTB10. These cell lines were compared with HeLa cells as a non-neuronal permissive cell culture model. Both of these neuronal cell lines were first cultured by Biedler *et al.* in the early 1970s. SH-SY5Y is a subclone of the HTB11 (SK-N-SH) neuroblastoma cell line that was selected as an apparently homogenous population of cells with neuronal cell morphology. HTB10 (also known as SK-N-MC), reported as a neuroepithelioma cell line, has been used as a model for different neurotrophic viruses, such as hepatitis C poliovirus [34, 35] and enterovirus A71 [36]. We used RNA sequencing (RNAseq) to determine the genes expressed in SH-SY5Y, HeLa and HTB10, and specifically assessed the expression of twenty-six neuronal cell marker genes that were selected from the Allen Brain Atlas [37-39] (http://brain-map.org) and from BioGPS [40, 41] (http://biogps.org) as being highly neuron-specific (**Table 1).** Of the 26 selected genes, 22 showed measurable expression in SH-SY5Y cells, 21 of which showed higher expression levels in SH-SY5Y compared to HTB10 cells, and little if any expression in HeLa cells. These findings support the use of SH-SY5Y as a model neuronal cell line, while raising questions about the suitability of HTB10 as a "neuronal-like" cell line.

Table 1. Expression of neuron-specific genes in HeLa, HTB10 and SH-SY5Y cell lines

Gene Symbol	Gene Name	HeLa	HTB10	SH-SY5Y
STMN2	stathmin 2	0.0[a]	0.0	1322.5
TCEAL7	transcription elongation factor A like 7	0.0	0.0	248.5
RGS4	regulator of G-protein signaling 4	0.0	0.0	163.7
NNAT	neuronatin	0.0	0.0	45.8
VIP	vasoactive intestinal peptide	0.0	0.0	39.3
TAGLN3	transgelin 3	0.0	0.0	39.0
SNAP25	synaptosome associated protein 25	1.8	0.7	24.6
LMO1	LIM domain only 1	0.6	0.0	17.0
CAMK2N1	calmodulin dependent protein kinase II inhibitor 1	1.2	0.0	11.8
SCG2	secretogranin II	0.0	0.0	10.7
CDO1	cysteine dioxygenase type 1	0.0	0.0	6.9
SLC10A4	solute carrier family 10 member 4	0.0	0.0	3.1
DLX5	distal-less homeobox 5	0.0	0.0	2.1
DBH	dopamine beta-hydroxylase	0.0	0.0	1.7
SYT17	synaptotagmin 17	0.1	0.0	1.1
CUX2	cut-like homeobox 2	0.0	0.1	1.1
CNTN4	contactin 4	0.0	0.2	1.0
DPYSL5	dihydropyrimidinase like 5	0.0	0.2	1.0
SV2C	synaptic vesicle glycoprotein 2C	0.0	0.0	0.7
ETV1	ETS variant 1	0.0	0.1	0.7
DCN	decorin	0.0	7.9	0.6
NXPH1	neurexophilin 1	0.0	0.0	0.1
FOXP2	forkhead box P2	0.2	2.2	0.0
GAD1	glutamate decarboxylase 1	0.0	0.2	0.0
NELL1	neural EGFL like 1	0.0	0.3	0.0
SLC17A7	solute carrier family 17 member 7	0.0	0.6	0.0

[a]Expression levels (transcripts per million reads – TPM) of 26 highly neuron-specific marker genes selected from the Allen Brain Atlas (http://brain-map.org) and BioGPS (http://biogps.org) were examined by RNA sequencing.

A representative B1 clade EV-D68 strain, US/MO/47, replicates in SH-SY5Y cells

Given the epidemiological association of recent EV-D68 infections with AFM, we sought to determine if there are any differential growth phenotypes between contemporary and historical EV-D68 strains in neuronal versus non-neuronal cell lines. To measure viral replication kinetics, each cell line was infected at a multiplicity of infection (MOI) of 0.1 and the virus growth was measured by determining virus titers ($TCID_{50}$) in culture supernatant at five time-points post-infection. To examine whether viruses from the B1 clade showed any phenotypic differences in their ability to infect human neuronal cells, we first selected three different viruses to represent the phylogenetic diversity of EV-D68. US/MO/14-18947 from Missouri (US/MO/47) was selected as a representative of the B1 clade since it carries all 21 substitutions identified in our previous comparative genomics analysis [22]. USA/N0051U5/2012 from Tennessee (US/TN) was selected as a representative of clade A since it was isolated in the U.S. during roughly the same timeframe as US/MO/47 and possesses none of the 21 substitutions. VR1197 was selected as an example of an historical isolate similar to the prototypical Fermon strain isolated in 1962.

All three EV-D68 strains replicate in the non-neuronal cell lines HeLa (**Fig 1A**) and the alveolar A549 cell line (**S1 Fig**). These viruses also cause cell death as judged by visual evidence of cytopathic effects (CPE) in infected cell culture (**Fig 1B**). In contrast, only the US/MO/47 could replicate in the SH-SY5Y neuronal cell line, reaching peak titers of ~10^5 $TCID_{50}$/ml by 48 hours post-infection (hpi). US/TN and VR1197 did not show any signs of replication, with titers not exceeding background after 96 hpi (**Fig 1A**). Similarly, CPE was observed after infection of SH-SY5Y cells with US/MO/47, but not with US/TN or

198 VR1197 (**Fig 1B**). Similar results were seen at MOIs of 0.01 and 1.0 (**S2 Fig**).
199 Furthermore, multiple passages of US/TN or VR1197 infected-supernatant onto fresh SH-
200 SY5Y cells (passaging every 4 days for 12 days) failed to produce CPE. No increase in
201 viral titers above background levels was detected by any virus following infection of
202 HTB10.
203
204 **Immunofluorescence confirms US/MO/47 replication in SH-SY5Y cells**
205 We also examined production of the virus VP1 protein during infection of HeLa and SH-
206 SY5Y cells. VP1 is among the initial proteins expressed following picornavirus infection,
207 preceding capsid assembly [42]. We examined the ability of US/MO/47, US/TN and
208 VR1197 viruses to synthesize the VP1 capsid protein 18 hpi using immunofluorescence.
209 VP1 protein was detected in cells following infection of HeLa cells with all three EV-D68
210 strains (**Fig 1C**). However, only the US/MO/47 isolate produced VP1 following infection
211 of the SH-SY5Y neuronal cell line (**Fig 1C**), which is consistent with our data on viral
212 replication and CPE (**Fig 1A and 1B**). Also consistent with the viral replication
213 experiments, no VP1 was produced by any of the three strains when HTB10 cells were
214 infected. As typically observed in picornaviruses, VP1 staining was observed in the
215 cytoplasm and not the nucleus of both HeLa and SH-SY5Y cells.
216
217 **Intramuscular virus injection of neurotropic EV-D68 causes paralysis in neonatal**
218 **mice**
219 US/MO/47, US/TN, and VR1197 were assessed *in vivo* for their ability to cause paralysis
220 and neuropathogenesis in two-day-old outbred Swiss Webster mouse pups as previously

221 described in Hixon *et. al* [21]. Intramuscular injection of US/MO/47 resulted in limb
222 paresis and paralysis in all mice injected (n=10) as quantified by a Motor Impairment
223 Score (**Fig 2A**) Materials. Most mice injected with US/MO/47 developed moderate to
224 severe paralysis in both rear limbs. Paralysis always began in the injected hind limb and
225 then spread to the contralateral hind limb in most animals, with rare spread of paralysis
226 to the fore limbs. Quantification of the average motor impairment over time showed onset
227 of weakness starting at approximately 4 days post-infection (dpi) with progressive
228 worsening through 7 dpi, with the majority of mice continuing to have moderate to severe
229 weakness in both hind limbs through the end of the observation period at 14 dpi. These
230 data are consistent with previously published results on EV-D68-induced paralysis [21,
231 43]. In contrast to US/MO/47, mice receiving intramuscular injection of US/TN (n=11) or
232 VR1197 (n=10) failed to develop any signs of motor impairment during the two-week
233 observation period.
234
235 **Neurotropic EV-D68 can be detected in the spinal cords of paralyzed mice**
236 Intramuscular infection with US/MO/47 resulted in increased titers of infectious virus
237 within mouse spinal cords paralleling the onset of motor impairment. Viral replication was
238 first detected at 2 dpi in spinal cords (~10^3 $TCID_{50}$/spinal cord), which corresponded with
239 a rapid increase in viral titer within the muscle tissue (~10^5 $TCID_{50}$/mg) of the injected limb
240 (Fig **2B**). Viral titer remained detectable in both spinal cords (~10^3 $TCID_{50}$/spinal cord)
241 and muscle tissue (~10^4 $TCID_{50}$/mg) at 6 dpi in US/MO/47-injected mice. In contrast,
242 neither US/TN or VR1197 produced detectable infection within mouse spinal cords. We
243 observed sustained viral titers from US/TN within mouse muscle up to 6 dpi (~10^3

244 $TCID_{50}$/mg), but no detectable spread of virus to spinal cord. VR1197 did not produce a
245 sustained infection in mouse muscle, and viral titer dropped to the limits of detection by 6
246 dpi.
247
248 **Replication kinetics of recently circulating EV-D68 strain in SH-SY5Y cell culture**
249 **model**
250 To further characterize the differential replication observed for diverse contemporary EV-
251 D68 isolates, and to test the SH-SY5Y cell infection mode, we obtained all additional
252 commercially available strains of EV-D68. These included strains from the B1, B2, and
253 D1 clades. Interestingly, all additional viral strains replicated in both HeLa and SH-SY5Y
254 (**3A Fig**), including another strain from the B1 clade, US/MO/49, a strain from the newly
255 defined D1 clade (US/KY), and a strain from the B2 clade (US/IL), replicating to a viral
256 titer of ~10^5 $TCID_{50}$/ml by 48 hpi. These three strains showed CPE after infection of SH-
257 SY5Y cells (**3D Fig)**. All EV-D68 strains replicated at similar rates in HeLa cells.
258
259 To validate our qualitative CPE evaluation, we performed an independent assay of cell
260 death using ATP content as determined by CellTiter Glo luminescence assay (Promega)
261 as a surrogate for viable, intact cells. Using a MOI of 0.1, cell viability dropped after 12
262 hpi when HeLa cells were infected with every EV-D68 strain tested and continued to drop
263 until the limit of detection was reached, between 48 and 72 hpi (**Fig 3B**). In contrast, cell
264 viability of infected SH-SY5Y cells, beginning at approximately 48 hpi, only dropped for
265 strains where CPE was present. The results of the cell viability and CPE assays was
266 reflective of the $TCID_{50}$ data in HeLa and SH-SY5Y cells for the new panel. The cell

viability assay was also performed at 37°C, which produced a similar replication pattern despite initials reports that EV-D68 grows poorly at 37°C [44]. We observed similar rates of viral replication in HeLa and SH-SY5Y cells at both 33°C and 37°C (**S3 Fig**).

Human Rhinovirus does not infect SH-SY5Y

SH-SY5Y cells were tested for infectivity across a broad selection of HRV strains: two strains from the HRV-B lineage (HRV-B6 and HRV-B14) and four strains from the HRV-A lineage (HRV-A95, HRV-A50, HRV-A36 and HRV-A20). Using the cell viability assay with a MOI of 0.1, the number of viable cells dropped for all HRV strains in HeLa cells. However, in SH-SY5Y cells, no evidence of HRV infectivity was observed for any strain tested using either the cell viability assay (**Fig 3C**) or visual inspection for CPE (**S4 Fig**).

Differential infection by EV-D68 viral strains is the same in differentiated and undifferentiated SH-SY5Y cells and in primary human neurons

To further characterize the differential replication capability of different EV-D68 strains, we differentiated SH-SY5Y using a well-established retinoic acid (RA) treatment protocol [45, 46], before virus infection, and confirmed differentiation by microscopic examination for morphological changes. We observed no difference in EV-D68 infectivity pattern between differentiated and undifferentiated SH-SY5Y cells. CPE observation and viral replication rate (**S5 Fig**) were similar compared to undifferentiated SH-SY5Y for all strains. All strains that could replicate in undifferentiated SH-SY5Y could also replicate in differentiated SH-SY5Y cells, and viral strains that could not replicate also did not replicate in differentiated SH-SY5Y cells. This demonstrates that EV-D68 strains are

capable of infecting neuronal precursors and can also infect mature differentiated neuronal cells. Primary human fetal brain-derived neurons were cultured and infected with US/TN, VR1197 and US/MO/47 (**S6 Fig**). Neurotropic and non-neurotropic EV-D68 strains showed the same infectivity pattern in SH-SY5Y. Using a MOI of 0.01, US/TN and VR1197 plated onto primary neuronal cells did not replicate and viral titers did not rise above the inoculation level baseline. In contrast, an increase in viral titers was observed when the neurotropic strain US/MO/47 infected primary neuronal cells and reached peak titer ~10^5 $TCID_{50}$/ml at 24 hpi.

All EV-D68 strains generate virus when transfected into SH-SY5Y cells

To determine if virus cell entry may be responsible for restricting virus replication in SH-SY5Y for some isolates, full-length genomic RNA from each of the EV-D68 isolates was transfected into the cytoplasm of SH-SY5Y cells and virus production was measured. RNA transfection into HeLa cells resulted in a viral infection and replication pattern similar to intact virus infections at a MOI of 0.1, with viral titers peaking at ~10^7 $TCID_{50}$/ml for all EV-D68 strains tested. In contrast to what we observed using standard infection assays, all tested D68 strains generated virus following RNA transfection into SH-SY5Y cells. However, the viral titer peaked at 10^4 $TCID_{50}$/ml 48 hours after transfection of SH-SY5Y for viral strains that could not infect SH-SY5Y cells using intact virions (**Fig 4**), whereas the viral titer continued to increase until saturation at approximately 10^7 $TCID_{50}$/ml following transfection of SH-SY5Y with strains that could infect SH-SY5Y cells.

313 **Discussion**

314

315 Here we report on the differential infectivity between various contemporary and historical
316 EV-D68 strains in SH-SY5Y as measured by viral replication, cell viability, CPE, and
317 immunofluorescence. The clade specificity of neuropathogenesis previously reported
318 [10, 22, 25-27, 32, 33] between contemporary and historical strains is observed in the
319 neurotropism in SH-SY5Y cells (**Figure 5**). Among the EV-D68 strains used in this study,
320 those from clades B1, B2 and D1 were able to infect SH-SY5Y cells and cause paralysis
321 in a mouse model, whereas those from clade A and other historical strains could not [47].
322 We also showed that this differential growth is at least partly due to differential viral entry,
323 as all strains can replicate and produce viral progeny after transfection.

324

325 To determine the most appropriate tissue culture model system, we explored the gene
326 expression by RNA sequencing and showed that transcripts from SH-SY5Y cells are
327 enriched for neuronal-specific genes relative to HeLa and HTB10 cells. This agrees with
328 several other groups which have shown the expression of specific neurological marker
329 genes in SH-SY5Y cells [45, 48, 49]. This neuronal cell line has successfully been used
330 as a model to study the *in vitro* neuropathogenic effects of different viruses, notably, as a
331 model for paralytic enteroviral isolates including EV-A71 and poliovirus [35, 50-56].
332 Numerous other viruses associated with neurological symptoms can infect SH-SY5Y,
333 including: Japanese encephalitis-virus [57], human immunodeficiency-virus [58], human
334 cytomegalovirus [59], varicella-zoster virus [60], chikungunya [61], mumps virus [62],

335 dengue virus [63], Zika virus [64, 65], and rabies virus [66] suggesting that SH-SY5Y is
336 an excellent model system for neurotropic viruses.

337

338 We found support of the biological relevance of SH-SY5Y cells as a cell culture model by
339 observing the same infectivity pattern *in vitro* with other neuronal cell cultures. SH-SY5Y
340 cells are capable of being differentiated using retinoic acid, which leads to more neuron-
341 specific morphology and gene expression. These differentiated cells are characterized
342 by the formation of extensive neurites, as well as the induction of neuron-specific
343 enzymes, receptors and neurotransmitters [45]. Differentiated SH-SY5Y cells have been
344 used as models for neuron-virus interactions [67] including EV-A71 [55, 56],
345 Chikungunya virus [61], and varicella-zoster virus [60]. Our results show that both
346 differentiated and undifferentiated SH-SY5Y can be infected with neurotropic strains of
347 EV-D68, suggesting neurotropic strains of EV-D68 can invade both immature and mature
348 neuronal cells. Primary human fetal brain-derived neurons have also been used to study
349 infectivity patterns of neurotropic viruses as well as the central nervous system [68, 69].
350 We also observed a similar EV-D68 replication pattern in human primary postnatal
351 neurons. Interestingly, despite initially reported as growing poorly at 37°C [44], we
352 observed similar rates of EV-D68 replication in SH-SY5Y cells at both 33°C and 37°C,
353 which would likely be a more biologically relevant temperature for paralytic infections at
354 the core body temperature rather than the lower temperature of the upper respiratory
355 system that supports more routine respiratory infection.

356

357 EV-D68 is closely related to human rhinovirus (HRV) within the *Picornaviridae* family [70].
358 Frequent coinfection in patients and cross-reactivity of nucleic acid amplification
359 screening had led to misdiagnosis of EV-D68 infection as HRV infection prior to the 2014
360 outbreak [71, 72]. Despite the similarity in respiratory symptoms, HRV lacks any
361 association with the neurological symptoms of other enteroviruses, such as EV-D68 and
362 EV-A71 [70]. Indeed, despite their similarity to EV-D68, none of the 6 HRV strains could
363 infect SH-SY5Y cells.

364

365 We hypothesized that the reason for differential replication in SH-SY5Y cells of EV-D68
366 strain relates to different viral entry capabilities. We used RNA transfection to deliver
367 infectious RNA to the cytoplasm, bypassing natural viral entry mechanisms during an
368 infection. All EV-D68 strains generated virus following RNA transfection, but in some
369 cases viral titers plateaued at a relatively lower level, suggesting that only a single round
370 of replication had occurred. HRV RNA transfected into SH-SY5Y cells produced a similar
371 result. Our interpretation is that differences in the sequence and structure of viral capsid
372 proteins are responsible for the differential infectivity in SH-SY5Y cells by EV-D68 strains,
373 and that viral entry is what prevents HRV, US/TN, and the historical strains from infecting
374 SH-SY5Y cells. It has recently been reported that a chimeric swap mutant exchanging
375 the viral capsid from EV-D68 VR1197 and a neurotropic EV-D94 strain capable of
376 replication in SH-SY5Y cells, results in a loss on infectivity in SH-SY5Y cells [47]. This
377 result further supports our conclusion that viral entry mediated by the capsid is the cause
378 of the observed differential neurotropism. Specific genetic residues may be the cause of
379 differential neurotropism. A comparative analysis using infectious clones bearing specific

polymorphisms will likely be needed to establish the determinants of neurotropism in SH-SY5Y. In particular, the 2014 outbreak B1 substitutions in VP1/98A, VP1/148V, VP1/280K, VP1/290S, VP1/308N, and VP2/222T are all located on the virion surface and could be directly involved in virus-host cell attachment and would be good candidates to evaluate.

Our results closely correlate with the differential paralytic myelitis caused by EV-D68 in mice suggesting that infectivity in SH-SY5Y cells may be an effective proxy for neuropathogenesis (**Figure 5**). Multiple contemporary EV-D68 strains that have been shown to cause paralytic myelitis in mice were also neurotropic in SH-SY5Y cells [21]. The historical, non-neurotropic strains that are nonparalytic in mice did not grow in SH-SY5Y cells. In particular, the contemporary EV-D68 strain, US/TN, which was non-neurotropic in SH-SY5Y cells and not previously reported in *Hixon et al*. failed to produce paralysis in mice and could not be found in mouse spinal cord tissue. US/TN appeared to replicate at a low level within mouse muscle tissue, indicating lack of paralysis was not due to an inability to infect the mice. The infectivity pattern in SH-SY5Y cells, along with the agreement in primary postnatal neurons, supports the mouse model reported in Hixon *et al.* [21] and validates the results in the SH-SY5Y human cell line. This is significant because, while useful, mouse models are costly and introduce potential caveats, such as transcriptional factor differences in mice versus humans [73-75] and is debated if the mouse model recapitulates human conditions [76, 77]. Evidence presented here supports the validity of the mouse model for further study of neurotropic EV-D68 viruses and the theory of a causal link between AFM in humans and EV-D68.

403 **Conclusion**

404 We present a differential neuronal infectivity phenotype between contemporary and
405 historical EV-D68 strains. Permissible infection of SH-SY5Y cells mimics the paralysis
406 pattern reported in animal models. The high throughput nature of tissue culture models
407 will allow for rapid screening of novel viral strains and recombinant viruses to elucidate
408 the genetic determinants of neurotropism and potential antiviral therapies. This can
409 enable identification of EV-D68 alleles responsible for neural infection and potentially
410 neurological disease and avoids the cost associated with large-scale screening using
411 animal models.

412 ## Materials and Methods

413 ### Ethics Statement

414 All studies were done in accordance with the University of Colorado IACUC and Animal
415 Use Committee (B-34716(03)1E). Mice were cared for in adherence to the National
416 Institute of Health (NIH) guidelines to the Care and Use of Laboratory Mice. Mouse pups
417 exhibiting paralysis were euthanized if unable to nurse. Mice were anaesthetized with
418 inhaled isoflurane before tissue collection or perfusion.

419

420 ### Cell culture

421 HeLa cells (ATCC) were maintained in Dulbecco's modified Eagle's medium (DMEM,
422 Gibco) supplemented with 10% fetal bovine serum (FBS, HyClone). HTB10 (ATCC) cells
423 were maintained in DMEM supplemented with 10% FBS and non-essential amino acids
424 (Gibco). SH-SY5Y (CLR-2266, ATCC) cells were maintained in a 1:1 mixture of DMEM
425 and F12 (Gibco) media supplemented with 10% FBS. To differentiate SH-SY5Y cells, a
426 ~50% confluent flask of SH-SY5Y cells had media replaced with 1:1 mixture of DMEM
427 and F12 (Gibco) media supplemented with 3% FBS and 10 μM retinoic acid (RA, Sigma)
428 [53]. After 3 d of exposure to RA, the morphology of cells was evaluated, and cells were
429 passaged for further use. Morphology and cytopathic effect was evaluated using an
430 inverted microscope. Human postnatal day 0 (P0) brain neurons were purchased from
431 ScienCell (Cat# 1520) and plated at a density of 40,000 neurons/well on poly-D-lysine
432 coated 96-well plates [69]. The neurons were maintained in ScienCell neuronal growth
433 media with penicillin-streptomycin (Cat# 1520) at 37ºC in 5% CO_2 until day in vitro (DIV)
434 7, by which time the neurons had well-established neurites.

435

436 **Virus Stock Preparation**

437 EV-D68 stocks were prepared by infecting HeLa or rhabdomyosarcoma cells (ATCC) at
438 33°C in 5% CO_2 until CPE was observed. Cell debris was removed by centrifugation and
439 titers determined in a standard Tissue Culture Infective Dose ($TCID_{50}$) assay and
440 calculated by the Spearman-Kärber method. The source of each strain is detailed in (**S1**
441 **table**)

442 **S1 Table: List of strains used in this study.**

Species	Strain name	Abbreviation	D68 clade	Accession #	Source
Enterovirus D68	USA/N0051U5/2012	US/TN	A	KT347280	Dr. Tina V. Hartert
Enterovirus D68	US/MO/14-18947	US/MO/47	B1	KM851225	ATCC VR-1823
Enterovirus D68	ATCC VR-1197	VR-1197	Fermon	KT725431	ATCC VR-1197
Enterovirus D68	US/IL/14-18952	US/IL	B2	KM851230	ATCC VR-1824
Enterovirus D68	US/KY/14-18953	US/KY	D1	KM851231	ATCC VR-1825
Enterovirus D68	US/MO/14-18949	US/MO/49	B1	KM851227	BEI NR-49130
Human Rhinovirus A	15-CV19	HRV-A20	N/A	JN614993	ATCC VR-495
Human Rhinovirus A	SF-998	HRV-A95	N/A	FJ445170	ATCC VR-1301
Human Rhinovirus A	A2#58	HRV-A50	N/A	FJ445135	ATCC VR-517
Human Rhinovirus A	342 H [V-171-001-021]	HRV-A36	N/A	JF781497	ATCC VR-1146
Human Rhinovirus B	1059	HRV-B14	N/A	NC_001490	ATCC VR-284
Human Rhinovirus B	Thompson	HRV-B6	N/A	JN614996	ATCC VR-486

443

444

445 **Replication kinetics of EV-D68.**

446 The replication kinetics for HeLa, A549, HTB10, SH-SY5Y and differentiated SH-SY5Y
447 cell were evaluated in a high throughput manner. Viral replication kinetics were measured
448 from sets of flat bottom 96-well plates. Sets of plates corresponding to the number of
449 desired timepoints in an experiment were infected at the same initial time, using distinct
450 96-well plates for each time point. Infected plates were incubated at 33-34°C, 5% CO_2
451 until the designated time point when each corresponding plate was placed in a -80°C
452 freezer until the entire time course was completed. Mock infected wells adjacent to each
453 condition demonstrated that no contamination occurred across wells. After 2 h, high MOI
454 conditions (0.1 and 1) were washed three times with phosphate buffered saline (PBS)
455 and the 2 h time point plate frozen to determine the background levels of virus present,
456 since 2 h is long enough for EV-D68 entry but not long enough for replication. After three
457 freeze-thaw cycles the viral titers from 10-fold serial dilutions of each sample were
458 evaluated using a 50% $TCID_{50}$ assay on HeLa cells. Plates were scored after adding 100
459 µl of crystal violet fixative per well followed by a 1 h incubation at room temperature (RT)
460 and washing to remove unbound dye. Crystal violet fixative was prepared by adding 5 g
461 crystal violet (sigma) and 8.5 g sodium chloride (Sigma) to 50 ml formaldehyde, 260 ml
462 ethanol, and 690 ml deionized water.

463

464 For replication kinetics in human postnatal neurons, day in-vitro (DIV) 7 neurons were
465 infected with EV-D68 US/MO/47, US/TN, or VR1197 at a MOI = 0.01. Infection media
466 was left on the cells for the duration of the experiment to minimize loss of cells from
467 multiple rinses due to low cell adhesion. Cell culture supernatant and lysate was collected

468 at 0, 6, 12, 24, 48, and 72 h, with three biological replicates collected per time point for
469 each viral strain. Lysate was serially-diluted 10-fold from 1 (raw lysate) to 10^{-6} RD cells at
470 33ºC and evaluated using a 50% $TCID_{50}$ assay.
471
472 **Immunostaining**
473 HeLa and SH-SY5Y cells were grown to 50-70% confluence on coverslips in a 24-well
474 plate and infected with EV-D68 strains at a MOI of 1.0. Mock infected cells serve as a
475 negative control. Coverslips were incubated at 34°C, 5% CO_2 for 18 hours, then fixed
476 with 4% paraformaldehyde (PFA) and stored at 4°C. The coverslips were washed with
477 PBS and cells were permeabilized with 0.1% Triton-X for 10 minutes. The coverslips
478 were blocked with 2% bovine serum albumin in PBS for 1 hour. The cells were incubated
479 with rabbit polyclonal α-VP1 of EV-D68 (GeneTex) at a final concentration of 4 µg/ml
480 overnight at 4°C, washed 3 times, and then incubated with a secondary goat α-rabbit
481 rhodamine red-X (Thermo Fisher) at a final concentration of 1 µg/ml for 30 minutes. To
482 visualize nuclei, DAPI stain was added to the second of three washes. The wells were
483 visualized on an Axioskop 2 plus (Zeiss) fluorescence microscope using DAPI and
484 Rhodamine filters. Images were taken with AxioCam MRc5 (Zeiss) camera using
485 AxioVision software. All images for a particular filter were taken under identical exposure
486 conditions.
487
488 **Mouse Infections with EV-D68**
489 Animal experiment were performed in an AAALAC accredited animal facility under IACUC
490 protocol B-34716(03)1E at the University of Colorado. Pregnant female Swiss Webster

mice were ordered from Envigo and kept in standard housing until the pups were born. At post-natal day 2, the dam and pups were transferred the BioSafety Level 2 (BSL2) region of the animal facility. P2 Swiss Webster mouse pups were then inoculated with $10^{6.8}$ TCID50/ml virus in 10 ul by intramuscular injection into the left medial hindlimb [21]. Mouse pups of both sexes were randomized to treatment conditions before virus inoculation.

Motor Impairment Scoring

Mice were monitored daily for 14 days. To assess paralysis, mice were removed from the cage and observed moving on a flat surface for several minutes in which each limb was given a motor impairment score: 0 - no motor impairment; 1 - mild motor impairment, ataxia or decreased movement present, toe/knuckle walking; 2 - moderate impairment, profound ataxia, limited movement of limb; 3 - severe impairment, no movement in limb, limb is non-weight bearing. The final motor impairment score for each day was achieved by summing the score for each limb.

Mouse tissue collection

Mouse pups were sacrificed by decapitation for collection of muscle and spinal cord tissue. Spinal cords were removed as previously described [21, 43]. Muscle tissue was collected from the inoculated limb (with the goal of obtaining as much muscle tissue possible from the anterior and posterior thigh and gastrocnemius). Both tissues were collected into BeadBug tubes containing inert ceramic bead and 0.3 mL of ice-cold, sterile PBS. Tissues were lysed mechanically on a BeadBug tissue homogenizer for 45 seconds

514 at 2800 rpm, and stored at -80°C. After thaw, tissue samples were spun at 2700xg for 1
515 minute to remove tissue chunks from the lysate. Lysate was serially-diluted 10-fold from
516 1 (raw lysate) to 10^{-6} and plated in a standard $TCID_{50}$ assay to determine the final viral
517 titer. To get the final titer per whole spinal cord, $TCID_{50}$/mL was multiplied by 0.3 mL. To
518 get the final muscle titer per milligram of tissue, $TCID_{50}$/mL was multiplied by 0.3 mL and
519 divided by the weight of tissue collected. Samples that were below the limit of detection
520 were graphed at zero.

521 **Cell ATP/viability assay.**

522 Cells were cultured and evaluated in the same manner as in the viral replication kinetics
523 assays. ATP levels were measured using the CellTiter-Glo luminescent cell viability
524 assay kit (catalog number G7570; Promega), and cell viability calculated relative to mock
525 control. To preserve the ATP levels so that each timepoint could be evaluated
526 concurrently, cell supernatant was removed and cells frozen at -80°C. Once the time
527 series was completed, all plates were removed and RT media was added to each plate.
528 Upon stabilization at RT for 20 min, the manufactures protocol was followed. We
529 validated this deviation from the manufactures protocol by confirming the linearity of the
530 assay across the active range of the study.

531

532 **RNA sequencing**

533 In order to explore the use of SH-SY5Y as an appropriate neuronal cell model, we used
534 RNA sequencing to obtain a comprehensive view of the genes expressed in SH-SY5Y,
535 HeLa and HTB10 cell lines. To prepare cells for RNA sequencing 10^4 cells were grown
536 in a 96 well plate for 24 h in quadruplicate before washing and resuspension in 10 µl of

Cell Lysis Buffer (0.2% Triton X-100, 2 Units/μL RNase inhibitor, 1:2,000,000 dilution of ERCC spike-in RNAs (Life Technologies)) per well. Full length cDNA was amplified using the SmartSeq2 protocol optimized in our laboratory [78, 79] before Nextera XT library preparation and sequencing on a NextSeq500 with 2 x 150 paired end reads. After adapter/primer trimming using the Trimmomatic tool (http://www.usadellab.org/cms/?page=trimmomatic), trimmed sequencing reads were mapped to transcripts derived from the human reference genome (GRCh37) and gene expression levels (transcripts per million reads) estimated using the RSEM package [80].

RNA purification and transfection

RNA used for transfections was purified from viral stocks grown in HeLa cells. Purification was performed using QIAamp MinElute Virus Spin Kit (Qiagen) according to the manufacturer's instructions; final RNA concentrations were approximately 100 ng/μl. In 12-well plates selected cell cultures were seeded and grown. According to the manufacturer's instructions, 200 ng of RNA was used with 2 μl of each reagent in the *Trans*IT®-mRNA transfection kit (Mirus) to perform a transfection.

Acknowledgements

We thank Dr. Tina V. Hartert and her colleagues at Vanderbilt for US/TN EV-D68 strain.

Figures Legends

559 **Fig 1. Differential infection and replication of EV-D68 strains in SH-SY5Y.** A) SH-
560 SY5Y, HTB10, and HeLa were grown to 90% confluence in 96-well plates before infection
561 with EV-D68 US/MO/47, US/TN and VR1197 at a MOI = 0.1. Infection media was
562 removed 2 hours post-infection (hpi) to reduce background. Cell culture lysates were
563 collected at various time points after infection, and viral titers measured using endpoint
564 dilutions for growth in HeLa cells. Dotted black line indicates the limit of detection. Error
565 bars represent SEM of three biological replicates. B) SH-SY5Y, HTB10, and HeLa were
566 infected with EV-D68 US/MO/47, US/TN and VR1197 at an MOI = 0.1 as above. Cells
567 were visualized at 72 hpi with bright field microscopy at 400x. C) HeLa and SH-SY5Y cell
568 lines were infected with the indicated EV-D68 strains at a MOI of 1.0. Cells were fixed at
569 18 hpi and stained with polyclonal antiserum against EV-D68 VP1 (red) and
570 counterstained with DAPI (blue) for nuclei detection.
571
572 **Fig 2. Differential motor impairment in mice following intramuscular injection.** A)
573 Motor impairment was scored daily for 14 days post-intramuscular challenges with the
574 indicated EV-D68 strains. None of the mice infected with US/TN or VR1197 mice
575 developed signs of paralysis, whereas 100% of mice infected with US/MO/47 developed
576 paralysis. Error bars represent standard error of the mean. B) Viral titers from muscle and
577 spinal cord titers were determined by $TCID_{50}$ assay on samples taken at 0, 2, 4, and 6
578 days post-intramuscular infection. Error bars represent the standard deviation.
579
580 **Fig 3. An expanded set of contemporary EV-D68 strains infect SH-SY5Y, but HRV**
581 **strains do not.** A) Hela and SH-SY5Y cells were infected with 6 different EV-D68 isolates

582 at a MOI of 0.1. Cell culture lysates were collected at various time points and viral titer
583 determined by $TCID_{50}$ in HeLa cells. Dotted black lines indicate the limit of detection.
584 Error bars represent SEM of three biological replicates. B) Similarly, cell viability was
585 determined by quantifying the ATP content of the supernatant with CellTiter Glo
586 (Promega) luminescence. Cell viability was calculated relative to mock-infected cultures.
587 Error bars represent SEM of three replicates. C) Six different human rhinovirus (HRV)
588 strains and two EV-D68 strains were used to infect HeLa and SH-SY5Y cell cultures at a
589 MOI of 0.1 and were visualized at 72 hpi. Cell viability was calculated as above. D)
590 Differential cytopathic effects of different EV-D68 isolates in HeLa and SH-SY5Y cells
591 after infection with different EV-D68 isolates at a MOI of 0.1 before visualization at 72 hpi.
592
593 **Fig 4. Replication of EV-D68 isolates following transfection of genomic RNA into**
594 **HeLa and SH-SY5Y cells.** RNAs were purified from various HRV and EV-D68 virus
595 stocks and used to transfect SH-SY5Y and HeLa cells. Cell culture lysates were collected
596 at various time points and viral titer determined by $TCID_{50}$ in HeLa cells. Error bars
597 represent SEM of three biological replicates.
598
599 **Fig 5. Phylogenetic tree of EV-D68 isolates based on VP1 sequences.** VP1 nucleotide
600 sequences of > 900 nt were retrieved from the ViPR site
601 (https://www.viprbrc.org/brc/home.spg?decorator=picorna_entero) on July 24, 2017.
602 Sequences were aligned using the MUSCLE algorithm and sequences showing poor
603 alignments were removed. A phylogenetic tree was computed using RaXML (bootstrap
604 replicates of 100) and then visualized using Archaeopteryx.js, via the ViPR site. Clade

605 classifications are based on bootstrap values of 100%. AFM-associated isolates are
606 marked with a green arrow. EV-D68 isolates used in this study are labeled either with a
607 pink (growth in SH-SY5Y cells) or orange (no growth in SH-SY5Y cells) arrow. Isolates
608 that are paralytogenic in mice (56) are labeled with a blue arrow.

609

610 **References**

611

612 1. Pallansch MA, Sandhu HS. The eradication of polio--progress and challenges. The New England
613 journal of medicine. 2006;355(24):2508-11. Epub 2006/12/15. doi: 10.1056/NEJMp068200.
614 PubMed PMID: 17167133.
615 2. CDC. AFM in the United States 2018 [cited 2018 March 20th 2018]. Available from:
616 https://www.cdc.gov/acute-flaccid-myelitis/afm-surveillance.html.
617 3. CDC. Epidemiology and Prevention of Vaccine-Preventable Diseases: National Center for
618 Immunization and Respiratory Diseases; 2015 [cited 2018 April 30th 2018]. Available from:
619 https://www.cdc.gov/vaccines/pubs/pinkbook/polio.html.
620 4. Schieble JH, Fox VL, Lennette EH. A probable new human picornavirus associated with
621 respiratory diseases. American journal of epidemiology. 1967;85(2):297-310. Epub 1967/03/01.
622 PubMed PMID: 4960233.
623 5. Khetsuriani N, Lamonte-Fowlkes A, Oberst S, Pallansch MA. Enterovirus surveillance--United
624 States, 1970-2005. Morbidity and mortality weekly report Surveillance summaries (Washington,
625 DC : 2002). 2006;55(8):1-20. Epub 2006/09/15. PubMed PMID: 16971890.
626 6. Imamura T, Oshitani H. Global reemergence of enterovirus D68 as an important pathogen for
627 acute respiratory infections. Rev Med Virol. 2015;25(2):102-14. doi: 10.1002/rmv.1820. PubMed
628 PMID: 25471236; PubMed Central PMCID: PMCPMC4407910.
629 7. Sejvar JJ, Lopez AS, Cortese MM, Leshem E, Pastula DM, Miller L, et al. Acute Flaccid Myelitis
630 in the United States, August-December 2014: Results of Nationwide Surveillance. Clin Infect
631 Dis. 2016;63(6):737-45. doi: 10.1093/cid/ciw372. PubMed PMID: 27318332.
632 8. Holm-Hansen CC, Midgley SE, Fischer TK. Global emergence of enterovirus D68: a systematic
633 review. The Lancet Infectious Diseases. 2016;16(5):e64-e75. doi: 10.1016/s1473-3099(15)00543-
634 5.
635 9. Ayscue P, Van Haren K, Sheriff H, Waubant E, Waldron P, Yagi S, et al. Acute flaccid paralysis
636 with anterior myelitis - California, June 2012-June 2014. MMWR Morbidity and mortality
637 weekly report. 2014;63(40):903-6. Epub 2014/10/10. PubMed PMID: 25299608.
638 10. Greninger AL, Naccache SN, Messacar K, Clayton A, Yu G, Somasekar S, et al. A novel
639 outbreak enterovirus D68 strain associated with acute flaccid myelitis cases in the USA (2012–
640 14): a retrospective cohort study. The Lancet Infectious Diseases. 2015;15(6):671-82. doi:
641 10.1016/s1473-3099(15)70093-9.
642 11. Messacar K, Schreiner TL, Van Haren K, Yang M, Glaser CA, Tyler KL, et al. Acute flaccid
643 myelitis: A clinical review of US cases 2012-2015. Ann Neurol. 2016;80(3):326-38. doi:
644 10.1002/ana.24730. PubMed PMID: 27422805; PubMed Central PMCID: PMCPMC5098271.
645 12. Messacar K, Schreiner TL, Maloney JA, Wallace A, Ludke J, Oberste MS, et al. A cluster of
646 acute flaccid paralysis and cranial nerve dysfunction temporally associated with an outbreak of

enterovirus D68 in children in Colorado, USA. The Lancet. 2015;385(9978):1662-71. doi: 10.1016/s0140-6736(14)62457-0.

13. Messacar K, Abzug MJ, Dominguez SR. 2014 outbreak of enterovirus D68 in North America. J Med Virol. 2016;88(5):739-45. doi: 10.1002/jmv.24410. PubMed PMID: 26489019.

14. Ng TF, Montmayeur A, Castro C, Cone M, Stringer J, Lamson DM, et al. Detection and Genomic Characterization of Enterovirus D68 in Respiratory Samples Isolated in the United States in 2016. Genome Announc. 2016;4(6). doi: 10.1128/genomeA.01350-16. PubMed PMID: 27932649; PubMed Central PMCID: PMCPMC5146441.

15. Lang M, Mirand A, Savy N, Henquell C, Maridet S, Perignon R, et al. Acute flaccid paralysis following enterovirus D68 associated pneumonia, France, 2014. Euro Surveill. 2014;19(44). Epub 2014/11/14. PubMed PMID: 25394254.

16. Bragstad K, Jakobsen K, Rojahn AE, Skram MK, Vainio K, Holberg-Petersen M, et al. High frequency of enterovirus D68 in children hospitalised with respiratory illness in Norway, autumn 2014. Influenza Other Respir Viruses. 2015;9(2):59-63. doi: 10.1111/irv.12300. PubMed PMID: 25534826; PubMed Central PMCID: PMCPMC4353317.

17. Yea C, Bitnun A, Robinson J, Mineyko A, Barton M, Mah JK, et al. Longitudinal Outcomes in the 2014 Acute Flaccid Paralysis Cluster in Canada. J Child Neurol. 2017;32(3):301-7. doi: 10.1177/0883073816680770. PubMed PMID: 28193112.

18. Levy A, Roberts J, Lang J, Tempone S, Kesson A, Dofai A, et al. Enterovirus D68 disease and molecular epidemiology in Australia. J Clin Virol. 2015;69:117-21. Epub 2015/07/26. doi: 10.1016/j.jcv.2015.06.079. PubMed PMID: 26209392.

19. Van Haren K, Ayscue P, Waubant E, Clayton A, Sheriff H, Yagi S, et al. Acute Flaccid Myelitis of Unknown Etiology in California, 2012-2015. JAMA. 2015;314(24):2663-71. doi: 10.1001/jama.2015.17275. PubMed PMID: 26720027.

20. Maloney JA, Mirsky DM, Messacar K, Dominguez SR, Schreiner T, Stence NV. MRI findings in children with acute flaccid paralysis and cranial nerve dysfunction occurring during the 2014 enterovirus D68 outbreak. AJNR Am J Neuroradiol. 2015;36(2):245-50. doi: 10.3174/ajnr.A4188. PubMed PMID: 25414005.

21. Hixon AM, Yu G, Leser JS, Yagi S, Clarke P, Chiu CY, et al. A mouse model of paralytic myelitis caused by enterovirus D68. PLoS Pathog. 2017;13(2):e1006199. doi: 10.1371/journal.ppat.1006199. PubMed PMID: 28231269; PubMed Central PMCID: PMCPMC5322875.

22. Zhang Y, Cao J, Zhang S, Lee AJ, Sun G, Larsen CN, et al. Genetic changes found in a distinct clade of Enterovirus D68 associated with paralysis during the 2014 outbreak. Virus Evol. 2016;2(1):vew015. doi: 10.1093/ve/vew015. PubMed PMID: 28512577; PubMed Central PMCID: PMCPMC5426007.

23. Drake JW. Rates of spontaneous mutation among RNA viruses. Proc Natl Acad Sci U S A. 1993;90(9):4171-5. Epub 1993/05/01. PubMed PMID: 8387212; PubMed Central PMCID: PMCPMC46468.

24. Lukashev AN, Lashkevich VA, Ivanova OE, Koroleva GA, Hinkkanen AE, Ilonen J. Recombination in circulating enteroviruses. J Virol. 2003;77(19):10423-31. Epub 2003/09/13. PubMed PMID: 12970427; PubMed Central PMCID: PMCPMC228507.

25. Gong YN, Yang SL, Shih SR, Huang YC, Chang PY, Huang CG, et al. Molecular evolution and the global reemergence of enterovirus D68 by genome-wide analysis. Medicine (Baltimore). 2016;95(31):e4416. doi: 10.1097/MD.0000000000004416. PubMed PMID: 27495059; PubMed Central PMCID: PMCPMC4979813.

26. Yip CCY, Lo JYC, Sridhar S, Lung DC, Luk S, Chan KH, et al. First Report of a Fatal Case Associated with EV-D68 Infection in Hong Kong and Emergence of an Interclade Recombinant in China Revealed by Genome Analysis. Int J Mol Sci. 2017;18(5). doi: 10.3390/ijms18051065. PubMed PMID: 28509856; PubMed Central PMCID: PMCPMC5454976.

27. Lau SK, Yip CC, Zhao PS, Chow WN, To KK, Wu AK, et al. Enterovirus D68 Infections Associated with Severe Respiratory Illness in Elderly Patients and Emergence of a Novel Clade in Hong Kong. Sci Rep. 2016;6:25147. doi: 10.1038/srep25147. PubMed PMID: 27121085; PubMed Central PMCID: PMCPMC4848506.
28. Xiang Z, Xie Z, Liu L, Ren L, Xiao Y, Paranhos-Baccala G, et al. Genetic divergence of enterovirus D68 in China and the United States. Sci Rep. 2016;6:27800. doi: 10.1038/srep27800. PubMed PMID: 27278628; PubMed Central PMCID: PMCPMC4899779.
29. Dyrdak R, Grabbe M, Hammas B, Ekwall J, Hansson KE, Luthander J, et al. Outbreak of enterovirus D68 of the new B3 lineage in Stockholm, Sweden, August to September 2016. Euro Surveill. 2016;21(46). Epub 2016/12/06. doi: 10.2807/1560-7917.es.2016.21.46.30403. PubMed PMID: 27918255; PubMed Central PMCID: PMCPMC5144949.
30. Knoester M, Scholvinck EH, Poelman R, Smit S, Vermont CL, Niesters HG, et al. Upsurge of Enterovirus D68, the Netherlands, 2016. Emerg Infect Dis. 2017;23(1):140-3. doi: 10.3201/eid2301.161313. PubMed PMID: 27660916; PubMed Central PMCID: PMCPMC5176244.
31. Wei HY, Yeh TK, Hsieh JY, Lin IP, Yang JY. Updates on the molecular epidemiology of Enterovirus D68 after installation of screening test among acute flaccid paralysis patients in Taiwan. Journal of microbiology, immunology, and infection = Wei mian yu gan ran za zhi. 2018. Epub 2018/01/18. doi: 10.1016/j.jmii.2017.12.001. PubMed PMID: 29339008.
32. Esposito S, Chidini G, Cinnante C, Napolitano L, Giannini A, Terranova L, et al. Acute flaccid myelitis associated with enterovirus-D68 infection in an otherwise healthy child. Virol J. 2017;14(1):4. doi: 10.1186/s12985-016-0678-0. PubMed PMID: 28081720; PubMed Central PMCID: PMCPMC5234096.
33. Wang G, Zhuge J, Huang W, Nolan SM, Gilrane VL, Yin C, et al. Enterovirus D68 Subclade B3 Strain Circulating and Causing an Outbreak in the United States in 2016. Sci Rep. 2017;7(1):1242. doi: 10.1038/s41598-017-01349-4. PubMed PMID: 28455514; PubMed Central PMCID: PMCPMC5430842.
34. De Jesus N, Franco D, Paul A, Wimmer E, Cello J. Mutation of a single conserved nucleotide between the cloverleaf and internal ribosome entry site attenuates poliovirus neurovirulence. J Virol. 2005;79(22):14235-43. Epub 2005/10/29. doi: 10.1128/jvi.79.22.14235-14243.2005. PubMed PMID: 16254358; PubMed Central PMCID: PMCPMC1280220.
35. Agol VI, Drozdov SG, Ivannikova TA, Kolesnikova MS, Korolev MB, Tolskaya EA. Restricted growth of attenuated poliovirus strains in cultured cells of a human neuroblastoma. J Virol. 1989;63(9):4034-8. Epub 1989/09/01. PubMed PMID: 2548013; PubMed Central PMCID: PMCPMC251001.
36. Chan SY, Sam IC, Lai JK, Chan YF. Cellular proteome alterations in response to enterovirus 71 and coxsackievirus A16 infections in neuronal and intestinal cell lines. Journal of proteomics. 2015;125:121-30. Epub 2015/05/25. doi: 10.1016/j.jprot.2015.05.016. PubMed PMID: 26003530.
37. Su AI, Wiltshire T, Batalov S, Lapp H, Ching KA, Block D, et al. A gene atlas of the mouse and human protein-encoding transcriptomes. Proc Natl Acad Sci U S A. 2004;101(16):6062-7. Epub 2004/04/13. doi: 10.1073/pnas.0400782101. PubMed PMID: 15075390; PubMed Central PMCID: PMCPMC395923.
38. Shen EH, Overly CC, Jones AR. The Allen Human Brain Atlas: comprehensive gene expression mapping of the human brain. Trends in neurosciences. 2012;35(12):711-4. Epub 2012/10/09. doi: 10.1016/j.tins.2012.09.005. PubMed PMID: 23041053.
39. Hawrylycz MJ, Lein ES, Guillozet-Bongaarts AL, Shen EH, Ng L, Miller JA, et al. An anatomically comprehensive atlas of the adult human brain transcriptome. Nature. 2012;489(7416):391-9. Epub 2012/09/22. doi: 10.1038/nature11405. PubMed PMID: 22996553; PubMed Central PMCID: PMCPMC4243026.

40. Wu C, Jin X, Tsueng G, Afrasiabi C, Su AI. BioGPS: building your own mash-up of gene annotations and expression profiles. Nucleic Acids Research. 2016;44(Database issue):D313-D6. doi: 10.1093/nar/gkv1104. PubMed PMID: PMC4702805.
41. Wu C, Orozco C, Boyer J, Leglise M, Goodale J, Batalov S, et al. BioGPS: an extensible and customizable portal for querying and organizing gene annotation resources. Genome Biology. 2009;10(11):R130-R. doi: 10.1186/gb-2009-10-11-r130. PubMed PMID: PMC3091323.
42. Li C, Wang JC, Taylor MW, Zlotnick A. In vitro assembly of an empty picornavirus capsid follows a dodecahedral path. J Virol. 2012;86(23):13062-9. Epub 2012/09/28. doi: 10.1128/jvi.01033-12. PubMed PMID: 23015694; PubMed Central PMCID: PMCPMC3497625.
43. Hixon AM, Clarke P, Tyler KL. Evaluating Treatment Efficacy in a Mouse Model of Enterovirus D68–Associated Paralytic Myelitis. The Journal of Infectious Diseases. 2017;216(10):1245-53. doi: 10.1093/infdis/jix468.
44. Oberste MS, Maher K, Schnurr D, Flemister MR, Lovchik JC, Peters H, et al. Enterovirus 68 is associated with respiratory illness and shares biological features with both the enteroviruses and the rhinoviruses. J Gen Virol. 2004;85(Pt 9):2577-84. Epub 2004/08/11. doi: 10.1099/vir.0.79925-0. PubMed PMID: 15302951.
45. Kovalevich J, Langford D. Considerations for the use of SH-SY5Y neuroblastoma cells in neurobiology. Methods in molecular biology (Clifton, NJ). 2013;1078:9-21. Epub 2013/08/27. doi: 10.1007/978-1-62703-640-5_2. PubMed PMID: 23975817; PubMed Central PMCID: PMCPMC5127451.
46. Pahlman S, Ruusala AI, Abrahamsson L, Mattsson ME, Esscher T. Retinoic acid-induced differentiation of cultured human neuroblastoma cells: a comparison with phorbolester-induced differentiation. Cell differentiation. 1984;14(2):135-44. Epub 1984/06/01. PubMed PMID: 6467378.
47. Royston L, Essaidi-Laziosi M, Pérez-Rodríguez FJ, Piuz I, Geiser J, Krause K-H, et al. Viral chimeras decrypt the role of enterovirus capsid proteins in viral tropism, acid sensitivity and optimal growth temperature. PLOS Pathogens. 2018;14(4):e1006962. doi: 10.1371/journal.ppat.1006962.
48. Lopes FM, Schroder R, da Frota ML, Jr., Zanotto-Filho A, Muller CB, Pires AS, et al. Comparison between proliferative and neuron-like SH-SY5Y cells as an in vitro model for Parkinson disease studies. Brain research. 2010;1337:85-94. Epub 2010/04/13. doi: 10.1016/j.brainres.2010.03.102. PubMed PMID: 20380819.
49. Biedler JL, Roffler-Tarlov S, Schachner M, Freedman LS. Multiple neurotransmitter synthesis by human neuroblastoma cell lines and clones. Cancer Res. 1978;38(11 Pt 1):3751-7. PubMed PMID: 29704.
50. Shastry P, Basu A, Rajadhyaksha MS. Neuroblastoma cell lines--a versatile in vitro model in neurobiology. The International journal of neuroscience. 2001;108(1-2):109-26. Epub 2001/05/01. doi: 10.3109/00207450108986509. PubMed PMID: 11328706.
51. Cordey S, Petty TJ, Schibler M, Martinez Y, Gerlach D, van Belle S, et al. Identification of site-specific adaptations conferring increased neural cell tropism during human enterovirus 71 infection. PLoS Pathog. 2012;8(7):e1002826. Epub 2012/08/23. doi: 10.1371/journal.ppat.1002826. PubMed PMID: 22910880; PubMed Central PMCID: PMCPMC3406088.
52. Kung CM, King CC, Lee CN, Huang LM, Lee PI, Kao CL. Differences in replication capacity between enterovirus 71 isolates obtained from patients with encephalitis and those obtained from patients with herpangina in Taiwan. J Med Virol. 2007;79(1):60-8. Epub 2006/11/30. doi: 10.1002/jmv.20761. PubMed PMID: 17133556.
53. Kok CC, Phuektes P, Bek E, McMinn PC. Modification of the untranslated regions of human enterovirus 71 impairs growth in a cell-specific manner. J Virol. 2012;86(1):542-52. Epub 2011/10/28. doi: 10.1128/jvi.00069-11. PubMed PMID: 22031931; PubMed Central PMCID: PMCPMC3255918.

54. La Monica N, Racaniello VR. Differences in replication of attenuated and neurovirulent polioviruses in human neuroblastoma cell line SH-SY5Y. J Virol. 1989;63(5):2357-60. Epub 1989/05/01. PubMed PMID: 2539524; PubMed Central PMCID: PMCPMC250657.
55. Ong KC, Wong KT. Understanding Enterovirus 71 Neuropathogenesis and Its Impact on Other Neurotropic Enteroviruses. Brain Pathol. 2015;25(5):614-24. doi: 10.1111/bpa.12279. PubMed PMID: 26276025.
56. Yogarajah T, Ong KC, Perera D, Wong KT. Enterovirus A71 and coxsackievirus A16 show different replication kinetics in human neuronal and non-neuronal cell lines. Arch Virol. 2017;162(3):727-37. doi: 10.1007/s00705-016-3157-4. PubMed PMID: 27878462.
57. Yun SI, Choi YJ, Song BH, Lee YM. 3' cis-acting elements that contribute to the competence and efficiency of Japanese encephalitis virus genome replication: functional importance of sequence duplications, deletions, and substitutions. J Virol. 2009;83(16):7909-30. Epub 2009/06/06. doi: 10.1128/jvi.02541-08. PubMed PMID: 19494005; PubMed Central PMCID: PMCPMC2715749.
58. Vesanen M, Salminen M, Wessman M, Lankinen H, Sistonen P, Vaheri A. Morphological differentiation of human SH-SY5Y neuroblastoma cells inhibits human immunodeficiency virus type 1 infection. J Gen Virol. 1994;75 (Pt 1):201-6. Epub 1994/01/01. doi: 10.1099/0022-1317-75-1-201. PubMed PMID: 8113728.
59. Luo MH, Fortunato EA. Long-term infection and shedding of human cytomegalovirus in T98G glioblastoma cells. J Virol. 2007;81(19):10424-36. Epub 2007/07/27. doi: 10.1128/jvi.00866-07. PubMed PMID: 17652378; PubMed Central PMCID: PMCPMC2045481.
60. Christensen J, Steain M, Slobedman B, Abendroth A. Differentiated neuroblastoma cells provide a highly efficient model for studies of productive varicella-zoster virus infection of neuronal cells. J Virol. 2011;85(16):8436-42. Epub 2011/06/03. doi: 10.1128/jvi.00515-11. PubMed PMID: 21632750; PubMed Central PMCID: PMCPMC3147949.
61. Dhanwani R, Khan M, Bhaskar AS, Singh R, Patro IK, Rao PV, et al. Characterization of Chikungunya virus infection in human neuroblastoma SH-SY5Y cells: role of apoptosis in neuronal cell death. Virus Res. 2012;163(2):563-72. Epub 2012/01/03. doi: 10.1016/j.virusres.2011.12.009. PubMed PMID: 22210004.
62. Santos-Lopez G, Cruz C, Pazos N, Vallejo V, Reyes-Leyva J, Tapia-Ramirez J. Two clones obtained from Urabe AM9 mumps virus vaccine differ in their replicative efficiency in neuroblastoma cells. Microbes and infection. 2006;8(2):332-9. Epub 2005/11/22. doi: 10.1016/j.micinf.2005.06.031. PubMed PMID: 16298153.
63. Castellanos JE, Neissa JI, Camacho SJ. Dengue virus induces apoptosis in SH-SY5Y human neuroblastoma cells. Biomedica : revista del Instituto Nacional de Salud. 2016;36(0):156-8. Epub 2016/09/14. doi: 10.7705/biomedica.v36i0.2984. PubMed PMID: 27622805.
64. Chan JF, Yip CC, Tsang JO, Tee KM, Cai JP, Chik KK, et al. Differential cell line susceptibility to the emerging Zika virus: implications for disease pathogenesis, non-vector-borne human transmission and animal reservoirs. Emerg Microbes Infect. 2016;5:e93. doi: 10.1038/emi.2016.99. PubMed PMID: 27553173; PubMed Central PMCID: PMCPMC5034105.
65. Sacramento CQ, de Melo GR, de Freitas CS, Rocha N, Hoelz LV, Miranda M, et al. The clinically approved antiviral drug sofosbuvir inhibits Zika virus replication. Sci Rep. 2017;7:40920. Epub 2017/01/18. doi: 10.1038/srep40920. PubMed PMID: 28098253; PubMed Central PMCID: PMCPMC5241873.
66. Ahmad W, Li Y, Guo Y, Wang X, Duan M, Guan Z, et al. Rabies virus co-localizes with early (Rab5) and late (Rab7) endosomal proteins in neuronal and SH-SY5Y cells. Virologica Sinica. 2017;32(3):207-15. Epub 2017/06/22. doi: 10.1007/s12250-017-3968-9. PubMed PMID: 28634871.
67. Shipley MM, Mangold CA, Kuny CV, Szpara ML. Differentiated Human SH-SY5Y Cells Provide a Reductionist Model of Herpes Simplex Virus 1 Neurotropism. J Virol. 2017;91(23). Epub 2017/09/29. doi: 10.1128/jvi.00958-17. PubMed PMID: 28956768; PubMed Central PMCID: PMCPMC5686721.

68. Michaelis M, Kleinschmidt MC, Doerr HW, Cinatl J, Jr. Minocycline inhibits West Nile virus replication and apoptosis in human neuronal cells. The Journal of antimicrobial chemotherapy. 2007;60(5):981-6. Epub 2007/09/18. doi: 10.1093/jac/dkm307. PubMed PMID: 17872917.
69. Watanabe S, Ohno S, Shirogane Y, Suzuki SO, Koga R, Yanagi Y. Measles virus mutants possessing the fusion protein with enhanced fusion activity spread effectively in neuronal cells, but not in other cells, without causing strong cytopathology. J Virol. 2015;89(5):2710-7. Epub 2014/12/19. doi: 10.1128/jvi.03346-14. PubMed PMID: 25520515; PubMed Central PMCID: PMCPMC4325728.
70. Tapparel C, Siegrist F, Petty TJ, Kaiser L. Picornavirus and enterovirus diversity with associated human diseases. Infect Genet Evol. 2013;14:282-93. doi: 10.1016/j.meegid.2012.10.016. PubMed PMID: 23201849.
71. Jaramillo-Gutierrez G, Benschop KS, Claas EC, de Jong AS, van Loon AM, Pas SD, et al. September through October 2010 multi-centre study in the Netherlands examining laboratory ability to detect enterovirus 68, an emerging respiratory pathogen. J Virol Methods. 2013;190(1-2):53-62. Epub 2013/03/06. doi: 10.1016/j.jviromet.2013.02.010. PubMed PMID: 23458694.
72. Clusters of acute respiratory illness associated with human enterovirus 68--Asia, Europe, and United States, 2008-2010. MMWR Morbidity and mortality weekly report. 2011;60(38):1301-4. Epub 2011/10/01. PubMed PMID: 21956405.
73. Cheng Y, Ma Z, Kim BH, Wu W, Cayting P, Boyle AP, et al. Principles of regulatory information conservation between mouse and human. Nature. 2014;515(7527):371-5. Epub 2014/11/21. doi: 10.1038/nature13985. PubMed PMID: 25409826; PubMed Central PMCID: PMCPMC4343047.
74. Odom DT, Dowell RD, Jacobsen ES, Gordon W, Danford TW, MacIsaac KD, et al. Tissue-specific transcriptional regulation has diverged significantly between human and mouse. Nature genetics. 2007;39(6):730-2. Epub 2007/05/29. doi: 10.1038/ng2047. PubMed PMID: 17529977; PubMed Central PMCID: PMCPMC3797512.
75. Lin S, Lin Y, Nery JR, Urich MA, Breschi A, Davis CA, et al. Comparison of the transcriptional landscapes between human and mouse tissues. Proc Natl Acad Sci U S A. 2014;111(48):17224-9. Epub 2014/11/22. doi: 10.1073/pnas.1413624111. PubMed PMID: 25413365; PubMed Central PMCID: PMCPMC4260565.
76. Seok J, Warren HS, Cuenca AG, Mindrinos MN, Baker HV, Xu W, et al. Genomic responses in mouse models poorly mimic human inflammatory diseases. Proceedings of the National Academy of Sciences of the United States of America. 2013;110(9):3507-12. doi: 10.1073/pnas.1222878110. PubMed PMID: PMC3587220.
77. Takao K, Miyakawa T. Genomic responses in mouse models greatly mimic human inflammatory diseases. Proceedings of the National Academy of Sciences of the United States of America. 2015;112(4):1167-72. doi: 10.1073/pnas.1401965111. PubMed PMID: PMC4313832.
78. Krishnaswami SR, Grindberg RV, Novotny M, Venepally P, Lacar B, Bhutani K, et al. Using single nuclei for RNA-seq to capture the transcriptome of postmortem neurons. Nature protocols. 2016;11(3):499-524. Epub 2016/02/20. doi: 10.1038/nprot.2016.015. PubMed PMID: 26890679; PubMed Central PMCID: PMCPMC4941947.
79. Grindberg RV, Yee-Greenbaum JL, McConnell MJ, Novotny M, O'Shaughnessy AL, Lambert GM, et al. RNA-sequencing from single nuclei. Proc Natl Acad Sci U S A. 2013;110(49):19802-7. Epub 2013/11/20. doi: 10.1073/pnas.1319700110. PubMed PMID: 24248345; PubMed Central PMCID: PMCPMC3856806.
80. Li B, Dewey CN. RSEM: accurate transcript quantification from RNA-Seq data with or without a reference genome. BMC bioinformatics. 2011;12:323. Epub 2011/08/06. doi: 10.1186/1471-2105-12-323. PubMed PMID: 21816040; PubMed Central PMCID: PMCPMC3163565.

Supporting Information

898

899 **S1 Table. List of strains used in this study.**

900

901 **S1 Fig. EV-D68 virus titers in A549 cells.** A549 cells were grown to 90% confluence in
902 96 well plates before infection with EV-D68 US/MO/47, US/TN and VR1197 EV-D68 at a
903 MOI = 0.1. Infection media was removed after 2 hpi to reduce background. Cell culture
904 lysate/supernatants were collected at various time points after infection, and viral titers
905 measured using endpoint dilutions for growth in HeLa cells. Dotted black line indicates
906 the limit of detection. Error bars represent SEM of three biological replicates.

907

908 **S2 Fig. EV-D68 virus titers in three different cell cultures with additional MOIs.**
909 Cells from three different cell lines – SH-SY5Y, HTB10, and HeLa were grown to 90%
910 confluence in 96 well plates before infection with EV-D68 US/MO/47, US/TN and VR1197
911 EV-D68 at a MOI = 1.0 and MOI = 0.01. Infection media was removed after 2 hpi to
912 reduce background from MOI = 1.0. Cell culture lysate/supernatants were collected at
913 various time points after infection, and viral titers measured using endpoint dilutions for
914 growth in HeLa cells. Dotted black line indicates the limit of detection. Error bars
915 represent SEM of three biological replicates.

916

917 **S3 Fig. Cell viability in cells infected with EV-D68 at 37°C.** Using replicate plates, cell
918 viability was measured by quantifying ATP content as determined by CellTiter Glo
919 (Promega) luminescence. Cell viability calculated relative to mock. Error bars represent
920 SEM of four replicates.

S4 Fig. HRV does not infect SH-SY5Y. Six different HRV strains and two EV-D68 strains were used to infect HeLa and SH-SY5Y cell cultures grown in a 96-well plate at a MOI of 0.1 before visualization at 72 hpi.

S5 Fig. EV-D68 virus titers in differentiated SH-SY5Y cells. Differentiated SH-SY5Y were infected with 6 different isolates of EV-D68 at a MOI of 0.1. Cell culture lysate/supernatants was collected at various time points. Viral titer was determined by $TCID_{50}$ in HeLa cells. Dotted black line indicates the limit of detection. Error bars represent SEM of three biological replicates. Error bars represent SEM of three replicates.

S6 Fig. EV-D68 strain growth in human postnatal cortical neurons. Human postnatal day 0 brain neurons were maintained to day 7 *in vitro* before infection with EV-D68 US/MO/47, US/TN, or VR1197 at a MOI = 0.01. Cell culture lysates/supernatant were collected at various times post viral infection, and viral titers were measured using endpoint dilutions for growth in RD cells. The x-axis indicates the limit of detection. Error bars represent SD of three biological replicates.

A

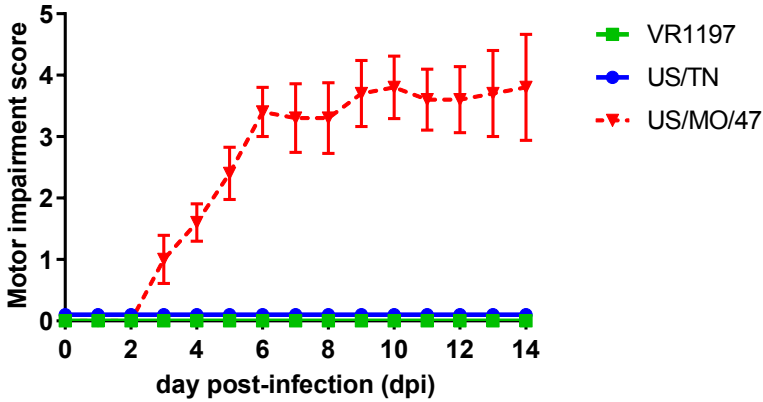
Motor impairment score
0
1
2
3
4
5
0
2
4
6
8
10
12
14
day post-infection (dpi)
VR1197
US/TN
US/MO/47

B

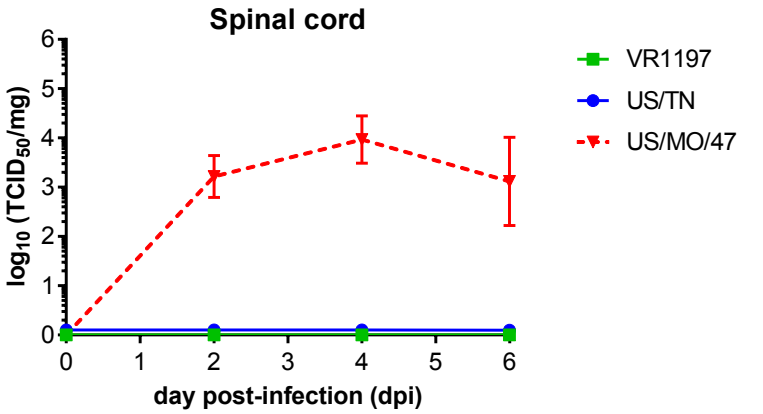
Spinal cord
log10 (TCID50/mg)
0
1
2
3
4
5
6
0
1
2
3
4
5
6
day post-infection (dpi)
VR1197
US/TN
US/MO/47

C

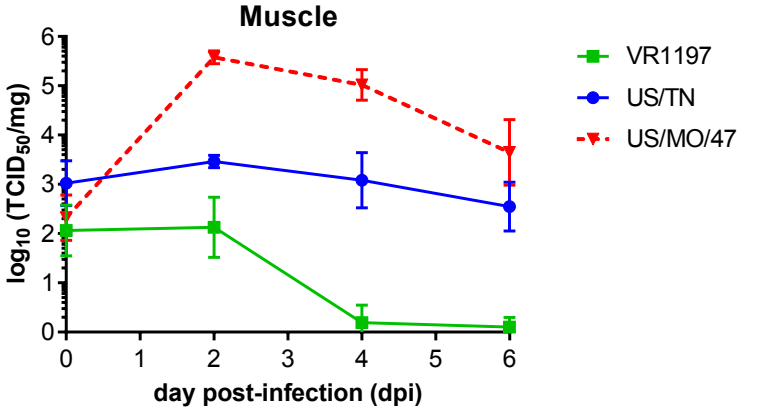
Muscle
log10 (TCID50/mg)
0
1
2
3
4
5
6
0
1
2
3
4
5
6
day post-infection (dpi)
VR1197
US/TN
US/MO/47

A

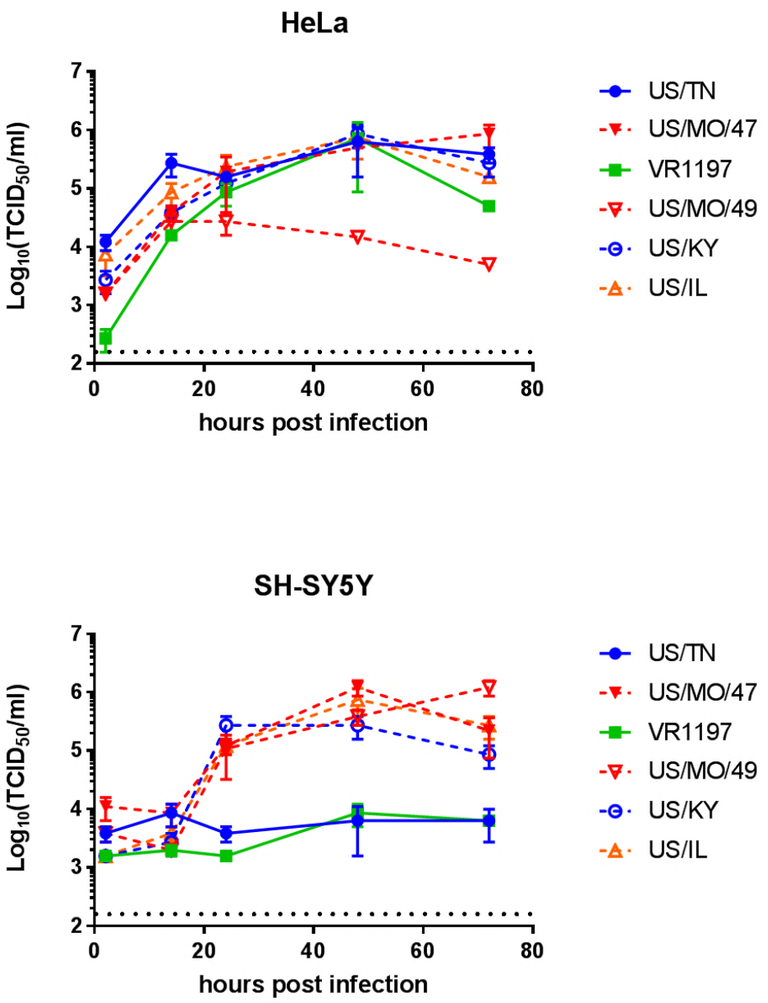

B

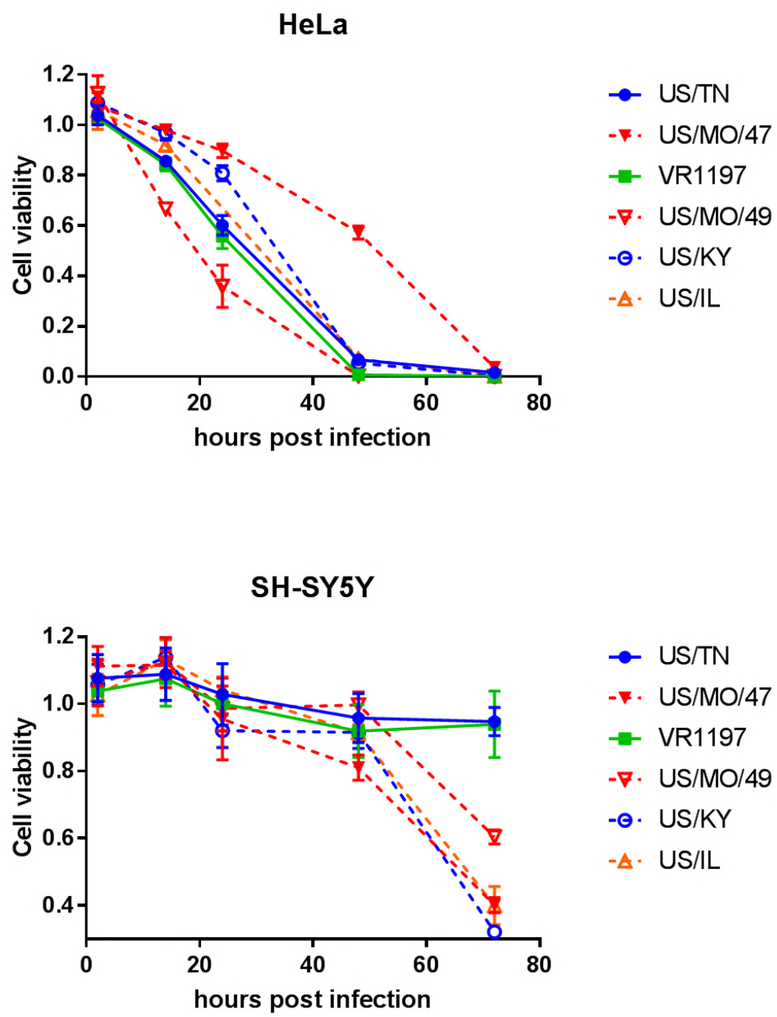

C

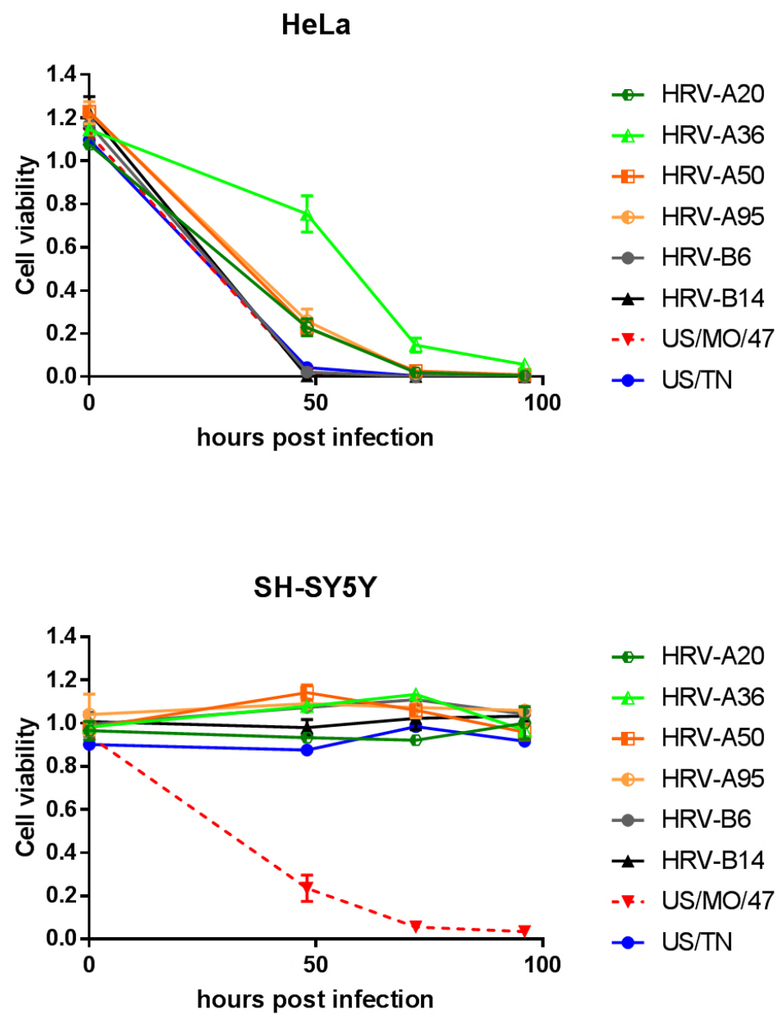

D

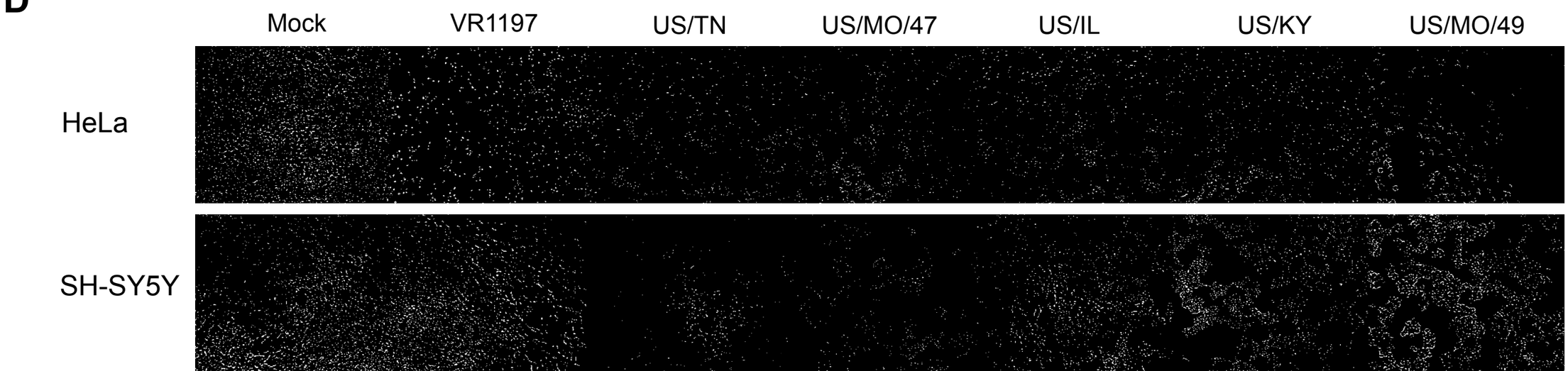

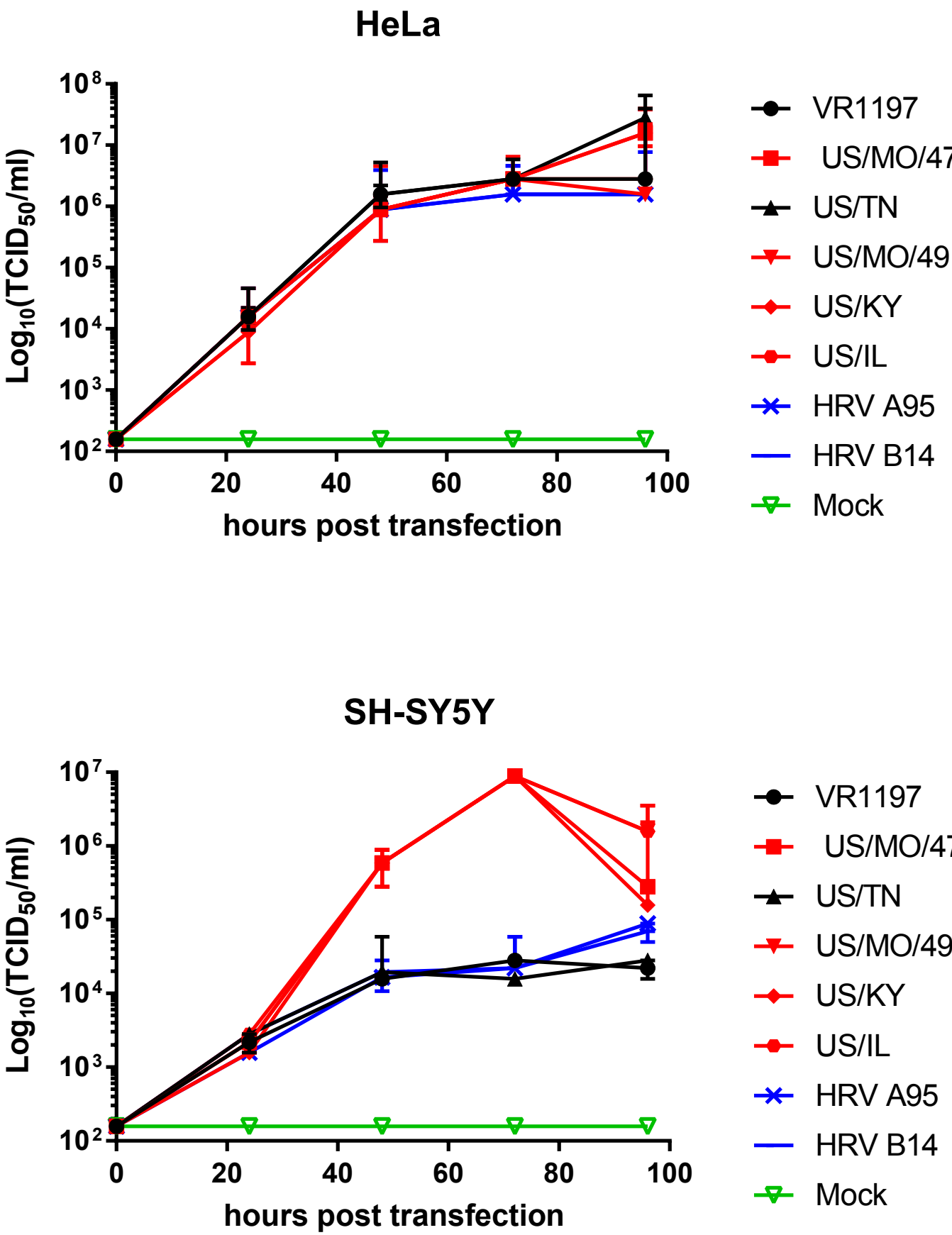
HeLa
Log10(TCID50/ml)
10^8
10^7
10^6
10^5
10^4
10^3
10^2
0
20
40
60
80
100
hours post transfection
VR1197
US/MO/47
US/TN
US/MO/49
US/KY
US/IL
HRV A95
HRV B14
Mock
SH-SY5Y
Log10(TCID50/ml)
10^7
10^6
10^5
10^4
10^3
10^2
0
20
40
60
80
100
hours post transfection
VR1197
US/MO/47
US/TN
US/MO/49
US/KY
US/IL
HRV A95
HRV B14
Mock

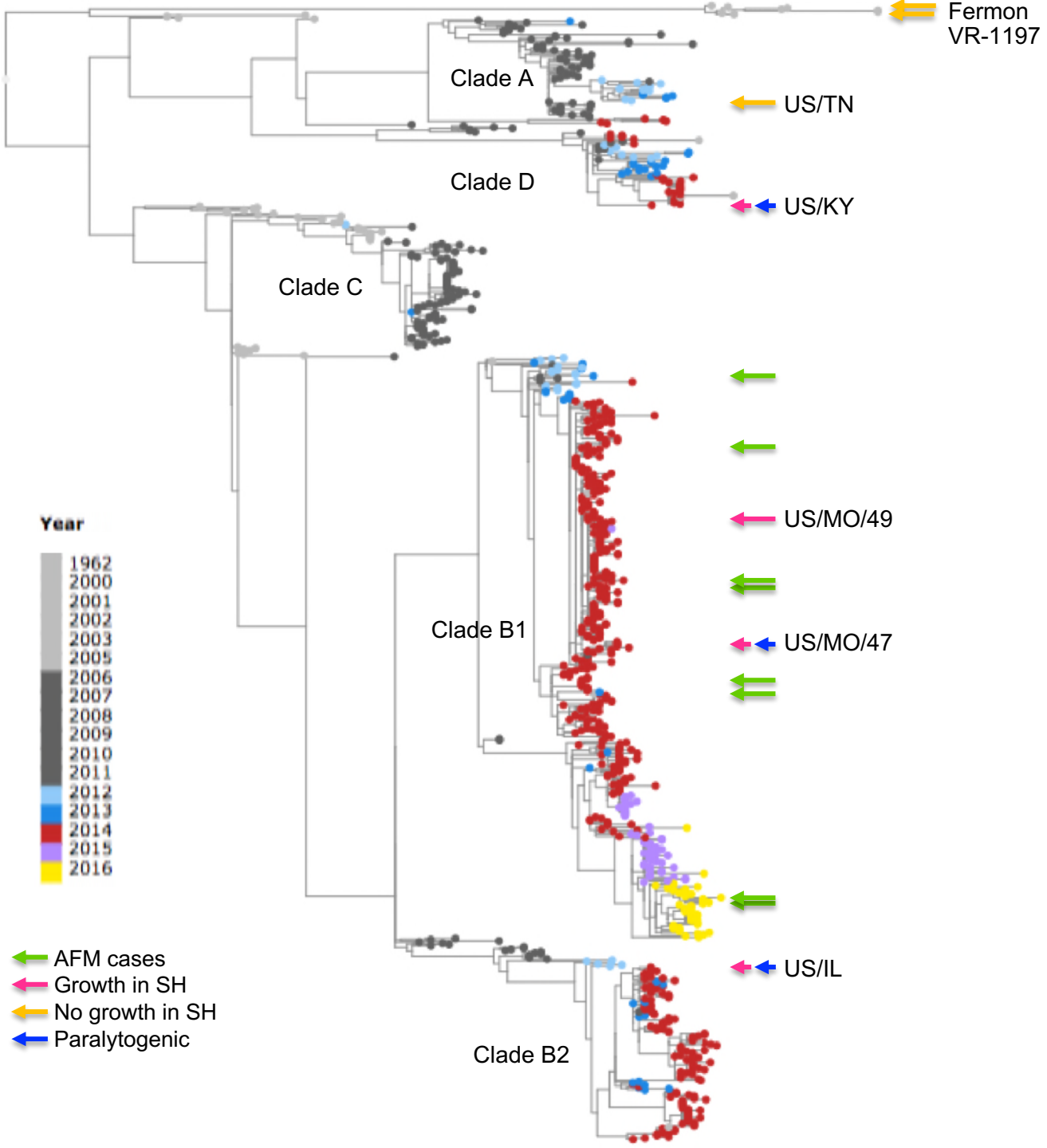
Fermon
VR-1197
Clade A
US/TN
Clade D
US/KY
Clade C
US/MO/49
Clade B1
US/MO/47
US/IL
Clade B2
Year
1962
2000
2001
2002
2003
2005
2006
2007
2008
2009
2010
2011
2012
2013
2014
2015
2016
AFM cases
Growth in SH
No growth in SH
Paralytogenic

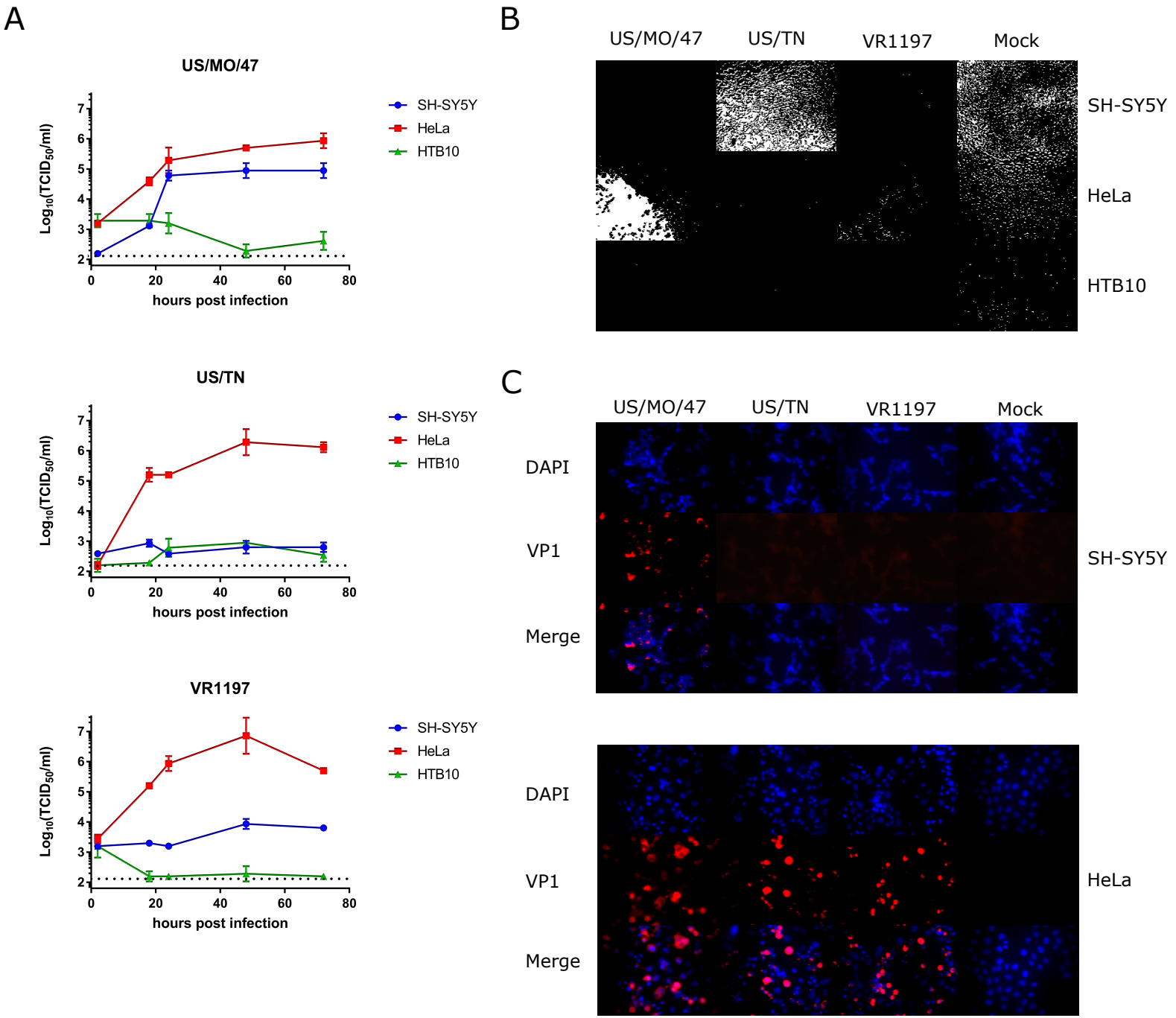
A
US/MO/47
Log10(TCID50/ml)
hours post infection
SH-SY5Y
HeLa
HTB10
US/TN
VR1197
B
US/MO/47
US/TN
VR1197
Mock
SH-SY5Y
HeLa
HTB10
C
DAPI
VP1
Merge